

# A REVISED CALIBRATION OF THE VIRIAL MASS ESTIMATOR FOR BLACK HOLES IN ACTIVE GALAXIES BASED ON SINGLE-EPOCH H $\beta$ SPECTRA

LUIS C. HO<sup>1,2</sup> AND MINJIN KIM<sup>3,4</sup>

*To appear in The Astrophysical Journal.*

## ABSTRACT

The masses of supermassive black holes in broad-line active galactic nuclei (AGNs) can be measured through reverberation mapping, but this method currently cannot be applied to very large samples or to high-redshift AGNs. As a practical alternative, one can devise empirical scaling relations, based on the correlation between broad-line region size and AGN luminosity and the relation between black hole mass and bulge stellar velocity dispersion, to estimate the virial masses of black holes from single-epoch spectroscopy. We present a revised calibration of the black hole mass estimator for the commonly used H $\beta$  emission line. Our new calibration takes into account the recent determination of the virial coefficient for pseudo and classical bulges.

*Subject headings:* galaxies: active — galaxies: nuclei — galaxies: Seyfert — quasars: emission lines — quasars: general

### 1. INTRODUCTION

Supermassive black holes (BHs) play a fundamental role in many aspects of contemporary extragalactic astronomy. However, direct methods to measure BH masses currently are limited to very nearby, largely inactive galaxies. Reverberation mapping (RM; Blandford & McKee 1982; Peterson 1993) of broad-line active galactic nuclei (AGNs) provides a means of measuring the size ( $R$ ) of their broad-line region (BLR), which, in combination with the velocity widths ( $\Delta V$ ) of the broad emission lines, yields a virial estimate of the BH mass

$$M_{\text{BH}}(\text{RM}) = f \frac{R(\Delta V)^2}{G}. \quad (1)$$

The virial coefficient  $f$  depends on the kinematics, geometry, and inclination of the BLR. In practice, it is set by normalizing the RM AGNs to the correlation between BH mass and bulge stellar velocity dispersion ( $M_{\text{BH}} - \sigma_*$  relation; Ferrarese & Merritt 2000; Gebhardt et al. 2000; see Kormendy & Ho 2013 for a review) established by local galaxies with direct BH mass measurements (e.g., Onken et al. 2004; Woo et al. 2010). Despite its utility, RM requires time-consuming, long-term spectroscopic monitoring, and, to date, only  $\sim 50$ , mostly nearby ( $z \lesssim 0.1$ ) AGNs have been studied in this manner (e.g., Peterson et al 2004; Barth et al. 2011; Grier et al. 2013). To access more luminous quasars and especially higher redshift systems, an alternative, much more expedient mass estimator can be devised from single-epoch spectroscopy by taking advantage of the empirical correlation between BLR size and continuum luminosity,  $R \propto L^\gamma$  (Kaspi et al. 2000), to estimate  $R$ . Then, from a straightforward measure of  $L$  and  $\Delta V$  from single-epoch or mean (time-averaged) spectra of the RM sample, one can solve for

$$\log M_{\text{BH}}(\text{RM}) = \log \text{VP}(\text{mean}) + a, \quad (2)$$

where  $a$  is a zero point offset and we define the virial product as

$$\text{VP}(\text{mean}) = \left( \frac{\Delta V}{1000 \text{ km s}^{-1}} \right)^2 \left( \frac{\lambda L_\lambda}{10^{44} \text{ erg s}^{-1}} \right)^\gamma. \quad (3)$$

The line width  $\Delta V$  can be parameterized as the full-width at half maximum (FWHM) or line dispersion ( $\sigma_{\text{line}}$ , second moment) of the broad line profile. The above approach to calibrate “single-epoch” spectra has been developed by a number of authors (e.g., McLure & Dunlop 2001; McLure & Jarvis 2002; Vestergaard 2002; Vestergaard & Peterson 2006; Wang et al. 2009). For lower redshift sources ( $z \lesssim 0.75$ ), the most commonly used emission line is H $\beta$ , and the continuum luminosity is referenced to 5100 Å.

Some recent developments justify a reassessment of the virial formalism to estimate BH masses from single-epoch H $\beta$  spectroscopy. Kormendy & Ho (2013) significantly updated the  $M_{\text{BH}} - \sigma_*$  relation for inactive galaxies, highlighting, in particular, the large and systematic differences between the relations for pseudo and classical bulges. This prompted Ho & Kim (2014) to calibrate the  $f$  factor separately for the two bulge types, using the latest sample of RM AGNs for which reliable bulge classifications could be performed. The changes are not negligible. Whereas previous studies obtained  $f \approx 4.2 - 5.5$  (Onken et al. 2004; Woo et al. 2010; Park et al. 2012; Grier et al. 2013), Ho & Kim find  $f = 6.3 \pm 1.5$  for classical bulges and ellipticals and  $f = 3.2 \pm 0.7$  for pseudobulges. (For the present discussion, we refer to  $f$  calculated using  $\Delta V = \sigma_{\text{line}}$ .) Apart from these revisions to the  $M_{\text{BH}} - \sigma_*$  relation and the new calibration of the  $f$  factor for pseudo and classical bulges, the  $R - L$  relation itself has been updated by Bentz et al. (2013).

### 2. CALIBRATION

Our new calibration of Equation 2 uses the updated database of properties for the RM AGNs and the bulge type classifications of their host galaxies given in Ho & Kim (2014), as summarized in Table 1. Specifically, we compute  $M_{\text{BH}}(\text{RM}) = f \text{VP}(\sigma_{\text{line}})$ , using  $f$  and  $\text{VP}(\sigma_{\text{line}})$  derived from root-mean-square (rms) spectra. We adopt  $f = 6.3 \pm 1.5$  for classical bulges

<sup>1</sup>Kavli Institute for Astronomy and Astrophysics, Peking University, Beijing 100871, China

<sup>2</sup>Department of Astronomy, School of Physics, Peking University, Beijing 100871, China

<sup>3</sup>Korea Astronomy and Space Science Institute, Daejeon 305-348, Republic of Korea

<sup>4</sup>University of Science and Technology, Daejeon 305-350, Republic of Korea

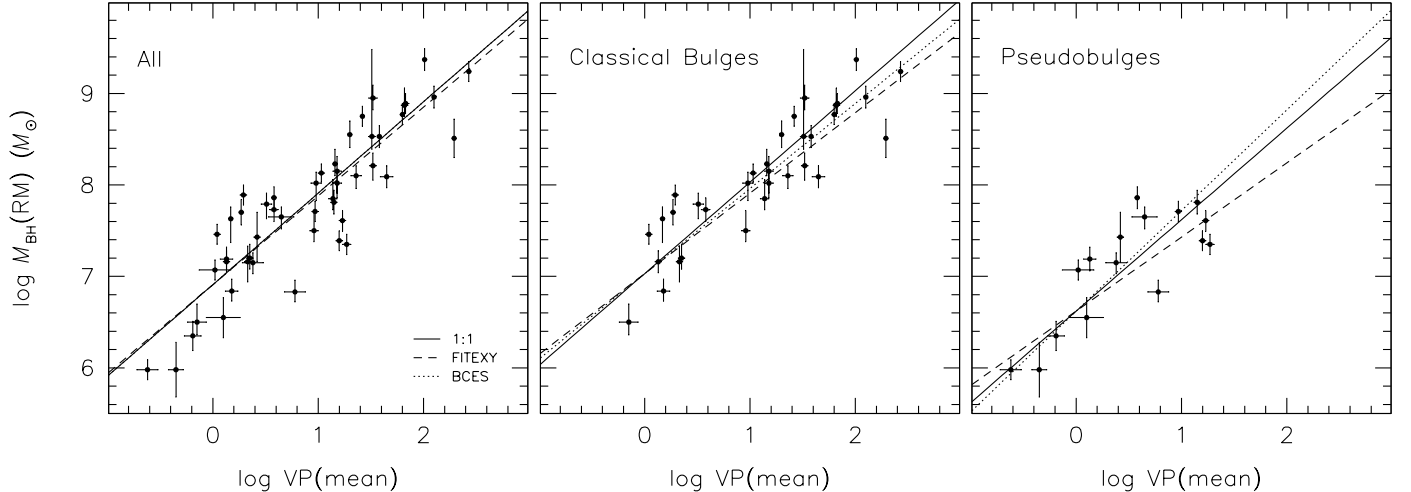


FIG. 1.— Comparison between RM BH masses and virial products calculated from FWHM of  $H\beta$  extracted from mean spectra for (left) the entire sample, (middle) classical bulges, and (right) pseudobulges. The solid line denotes a slope of unity, while the dashed and dotted lines give the regression based on the FITEXY and BCES fits, respectively.

and ellipticals and  $f = 3.2 \pm 0.7$  for pseudobulges. As an approximation to quantities pertaining to single-epoch spectra, we use the values of  $\lambda L_\lambda(5100 \text{ \AA})$  and  $\text{FWHM}(H\beta)$  derived from mean spectra, as listed in Table 2 of Ho & Kim (2014). Of the 43 RM AGNs that have bulge type classifications, 38 have available  $H\beta$  line widths extracted from mean spectra, among them 14 pseudo and 24 classical bulges. Among the empirical several criteria recommended by Kormendy & Ho (2013; see their Supplemental Material) to distinguish pseudobulges from classical bulges, we adopt, whenever possible, the most widely used condition: Sérsic (1968) index  $n < 2$ . However, the Sérsic index of the bulge can be difficult to measure accurately in the presence of a bright nucleus. Under these circumstances, Ho & Kim (2014) use a surrogate, equally effective criterion, that the bulge-to-total light fraction should be  $\lesssim 1/3$ . Six objects have more than one set of observations; in our analysis we treat these multiple data points as independent measurements. We have verified that combining the multiple measurements as a weighted average does not alter our final conclusions.

Figure 1 confirms that  $M_{\text{BH}}(\text{RM})$  correlates tightly and linearly with  $\text{VP}(\text{mean})$ . A linear regression using the FITEXY estimator (Press et al. 1992, as modified by Tremaine et al. 2002) yields a formal slope of  $0.97 \pm 0.07$  and an intrinsic scatter of 0.35 dex for the entire sample with both bulge types combined. The BCES algorithm of Akritas & Bershady (1996) gives a consistent slope of  $1.00 \pm 0.10$ . The middle and right panels of the figure show the correlations for the two bulge types separately. Although the FITEXY fit seems to suggest that pseudobulges have a slope less than unity, this is not supported by the BCES fit. Overall there is no evidence that the two bulge types behave differently.

Adopting a slope of  $\gamma = 0.533^{+0.035}_{-0.033}$  for the latest  $R-L$  relation (Bentz et al. 2013), the final mass scaling relation becomes

$$\log M_{\text{BH}}(H\beta) = \log \left[ \left( \frac{\text{FWHM}(H\beta)}{1000 \text{ km s}^{-1}} \right)^2 \left( \frac{\lambda L_\lambda(5100)}{10^{44} \text{ erg s}^{-1}} \right)^{0.533} \right] + a, \quad (4)$$

where  $a = 7.03 \pm 0.02$  for classical bulges and  $a = 6.62 \pm 0.04$  for pseudobulges, with a corresponding intrinsic scatter of 0.32

and 0.38 dex. For both bulge types combined,  $a = 6.91 \pm 0.02$  with an intrinsic scatter of 0.35 dex, essentially identical to the results of Vestergaard & Peterson (2006). It is remarkable that our new fit, which is based on a larger sample and significant updates to all of the RM and velocity dispersion data, turns out to be so similar to that of Vestergaard & Peterson published almost a decade ago. This may indicate that this type of calibration is still currently dominated by systematic effects (e.g., intrinsic differences in the factor  $f$ ).

### 3. CONCLUDING REMARKS

We present a new calibration of the prescription for estimating BH masses for broad-line AGNs and quasars using single-epoch spectra of the  $H\beta$  emission line. The primary difference between this and the previous work of Vestergaard & Peterson (2006) is that we account for the systematic difference in the virial coefficient  $f$  between pseudo and classical bulges (Ho & Kim 2014). We explicitly assume that AGNs hosted by pseudobulges follow a different  $M_{\text{BH}} - \sigma_*$  relation than those hosted by classical bulges, as observed in inactive galaxies. In addition, our calibration sample of RM AGNs is significantly larger and more current than that used by Vestergaard & Peterson, which was based on the sample of Peterson et al. (2004) from a decade ago. Incorporating also recent minor changes to the  $R-L$  relation, we find that the zero point of the  $H\beta$  virial mass formalism for classical bulges is a factor of 2.6 (0.41 dex) higher than that for pseudobulges. The commonly used  $H\beta$  calibration of Vestergaard & Peterson (2006) is very similar to ours for classical bulges, but their zero point is a factor of 2 higher than our zero point for pseudobulges.

This important source of systematic uncertainty obviously should be eliminated to the extent possible. However, as discussed in Ho & Kim (2014), in practice this will prove challenging because of the difficulty of measuring accurate host galaxy parameters for luminous, and especially distant, AGNs. As a general rule of thumb, any system with  $M_{\text{BH}} \gtrsim 10^8 M_\odot$  can be safely regarded as a classical bulge or elliptical galaxy. This can be seen from the distribution of BH masses in inactive galaxies (Ho & Kim 2014, Fig. 2), as well as for the RM-mapped AGNs in this paper (right panel of Fig. 1). At the other extreme, BHs

with  $M_{\text{BH}} \lesssim 10^6 M_{\odot}$  almost certainly reside in pseudobulges (e.g., Greene et al. 2008; Jiang et al. 2011). Between these two limiting cases ( $M_{\text{BH}} \approx 10^6 - 10^8 M_{\odot}$ ), BH masses estimated from single-epoch spectroscopy presently cannot be known to better than a factor of  $\sim 2$  without knowledge of the bulge type of the host galaxy.

We thank the referee for valuable criticisms. LCH acknowledges support by the Chinese Academy of Science through grant No. XDB09030102 (Emergence of Cosmological Structures) from the Strategic Priority Research Program and by the National Natural Science Foundation of China through grant No. 11473002.

## REFERENCES

- Akritas, M. G., & Bershadsky, M. A. 1996, *ApJ*, 470, 706  
 Barth, A. J., Pancoast, A., Thorman, S. J., et al. 2011, *ApJ*, 743, L4  
 Bentz, M. C., Denney, K. D., Grier, C. J., et al. 2013, *ApJ*, 767, 149  
 Blandford, R. D., & McKee, C. F. 1982, *ApJ*, 255, 419  
 Ferrarese, L., & Merritt, D. 2000, *ApJ*, 539, L9  
 Gebhardt, K., Bender, R., Bower, G., et al. 2000, *ApJ*, 539, L13  
 Greene, J. E., Ho, L. C., & Barth, A. J. 2008, *ApJ*, 688, 159  
 Grier, C. J., Martini, P., Watson, L. C., et al. 2013, *ApJ*, 773, 90  
 Ho, L. C., & Kim, M. 2014, *ApJ*, 789, 17  
 Jiang, Y.-F., Greene, J. E., Ho, L. C., Xiao, T., & Barth, A. J. 2011, *ApJ*, 742, 68  
 Kaspi, S., Smith, P. S., Netzer, H., et al. 2000, *ApJ*, 533, 631  
 Kormendy, J., & Ho, L. C. 2013, *ARA&A*, 51, 551  
 McLure, R. J., & Dunlop, J. S. 2001, *MNRAS*, 327, 199  
 McLure, R. J., & Jarvis, M. J. 2002, *MNRAS*, 337, 109  
 Onken, C. A., Ferrarese, L., Merritt, D., et al. 2004, *ApJ*, 615, 645  
 Park, D., Kelly, B. C., Woo, J.-H., & Treu, T. 2012, *ApJS*, 203, 6  
 Peterson, B. M. 1993, *PASP*, 105, 247  
 Peterson, B. M., Ferrarese, L., Gilbert, K. M., et al. 2004, *ApJ*, 613, 682  
 Press, W. H., Teukolsky, S. A., Vetterling, W. T., & Flannery, B. P. 1992, *Numerical Recipes in C: The Art of Scientific Computing* (2nd ed.; Cambridge: Cambridge Univ. Press)  
 Sérsic, J. L. 1968, *Atlas de Galaxias Australes* (Córdoba: Obs. Astron., Univ. Nac. Córdoba)  
 Tremaine, S., Gebhardt, K., Bender, R., et al. 2002, *ApJ*, 574, 740  
 Vestergaard, M. 2002, *ApJ*, 571, 733  
 Vestergaard, M., & Peterson, B. M. 2006, *ApJ*, 641, 689  
 Wang, J.-G., Dong, X.-B., Wang, T.-G., et al. 2009, *ApJ*, 707, 1334  
 Woo, J.-H., Treu, T., Barth, A. J., et al. 2010, *ApJ*, 716, 269

TABLE 1: SAMPLE OF REVERBERATION-MAPPED AGNS

Name	$\log \lambda L_{\lambda}(5100 \text{ \AA})$ ( $\text{erg s}^{-1}$ )	FWHM(mean) ( $\text{km s}^{-1}$ )	$\log \text{VP}(\text{mean})$ ( $M_{\odot}$ )	$\log M_{\text{BH}}(\text{RM})$ ( $M_{\odot}$ )	Bulge Type
(1)	(2)	(3)	(4)	(5)	(6)
3C 120	43.96±0.06	1430±16	0.29 <sup>+0.03</sup> <sub>-0.03</sub>	7.89 <sup>+0.11</sup> <sub>-0.11</sub>	CB
3C 390.3	44.36±0.03	13211±28	2.43 <sup>+0.12</sup> <sub>-0.02</sub>	9.24 <sup>+0.11</sup> <sub>-0.11</sub>	CB
Ark 120	43.92±0.06	6042±35	1.52 <sup>+0.03</sup> <sub>-0.03</sub>	8.21 <sup>+0.14</sup> <sub>-0.16</sub>	CB
	43.57±0.10	6246±78	1.36 <sup>+0.05</sup> <sub>-0.05</sub>	8.10 <sup>+0.11</sup> <sub>-0.14</sub>	CB
Arp 151	42.50±0.11	3098±69	0.18 <sup>+0.06</sup> <sub>-0.06</sub>	6.84 <sup>+0.13</sup> <sub>-0.11</sub>	CB
Fairall 9	43.92±0.05	6000±66	1.51 <sup>+0.03</sup> <sub>-0.03</sub>	8.53 <sup>+0.95</sup> <sub>-0.14</sub>	CB
Mrk 79	43.57±0.07	5056±85	1.18 <sup>+0.04</sup> <sub>-0.04</sub>	8.15 <sup>+0.16</sup> <sub>-0.29</sub>	CB
	43.67±0.07	4760±31	1.18 <sup>+0.04</sup> <sub>-0.04</sub>	8.02 <sup>+0.11</sup> <sub>-0.11</sub>	CB
	43.60±0.07	4766±71	1.14 <sup>+0.04</sup> <sub>-0.04</sub>	7.85 <sup>+0.21</sup> <sub>-0.12</sub>	CB
Mrk 202	42.21±0.18	1471±18	-0.62 <sup>+0.10</sup> <sub>-0.10</sub>	5.98 <sup>+0.11</sup> <sub>-0.11</sub>	PB
Mrk 509	44.13±0.05	3015±2	1.03 <sup>+0.03</sup> <sub>-0.03</sub>	8.13 <sup>+0.10</sup> <sub>-0.10</sub>	CB
Mrk 590	43.07±0.11	3729±426	0.65 <sup>+0.12</sup> <sub>-0.12</sub>	7.65 <sup>+0.11</sup> <sub>-0.13</sub>	PB
	43.32±0.08	2744±79	0.51 <sup>+0.05</sup> <sub>-0.05</sub>	7.79 <sup>+0.12</sup> <sub>-0.16</sub>	CB
	43.59±0.06	2500±43	0.58 <sup>+0.04</sup> <sub>-0.04</sub>	7.73 <sup>+0.13</sup> <sub>-0.13</sub>	CB
Mrk 1310	42.28±0.17	2409±24	-0.15 <sup>+0.09</sup> <sub>-0.09</sub>	6.50 <sup>+0.20</sup> <sub>-0.14</sub>	CB
NGC 3227	42.36±0.03	4445±134	0.42 <sup>+0.03</sup> <sub>-0.03</sub>	7.43 <sup>+0.27</sup> <sub>-0.27</sub>	PB
NGC 3783	42.55±0.18	3770±68	0.38 <sup>+0.10</sup> <sub>-0.10</sub>	7.15 <sup>+0.11</sup> <sub>-0.12</sub>	PB
NGC 4253	42.57±0.13	1609±39	-0.35 <sup>+0.07</sup> <sub>-0.07</sub>	5.98 <sup>+0.30</sup> <sub>-0.30</sub>	PB
NGC 4593	42.79±0.18	5143±16	0.78 <sup>+0.10</sup> <sub>-0.10</sub>	6.83 <sup>+0.13</sup> <sub>-0.11</sub>	PB
NGC 4748	42.55±0.13	1947±66	-0.19 <sup>+0.08</sup> <sub>-0.08</sub>	6.35 <sup>+0.16</sup> <sub>-0.16</sub>	PB
NGC 5548	42.95±0.11	12771±71	1.65 <sup>+0.06</sup> <sub>-0.06</sub>	8.09 <sup>+0.12</sup> <sub>-0.12</sub>	CB
NGC 6814	42.08±0.29	3323±7	0.02 <sup>+0.15</sup> <sub>-0.15</sub>	7.07 <sup>+0.11</sup> <sub>-0.11</sub>	PB
NGC 7469	43.36±0.10	1722±30	0.13 <sup>+0.06</sup> <sub>-0.06</sub>	7.19 <sup>+0.13</sup> <sub>-0.13</sub>	PB
PG 0003+199	43.70±0.06	1792±3	0.35 <sup>+0.03</sup> <sub>-0.03</sub>	7.20 <sup>+0.15</sup> <sub>-0.12</sub>	CB
	43.78±0.05	1679±2	0.33 <sup>+0.03</sup> <sub>-0.03</sub>	7.16 <sup>+0.17</sup> <sub>-0.22</sub>	CB
	43.68±0.06	1273±3	0.04 <sup>+0.03</sup> <sub>-0.03</sub>	7.46 <sup>+0.11</sup> <sub>-0.11</sub>	CB
PG 0026+129	44.91±0.02	2544±56	1.30 <sup>+0.02</sup> <sub>-0.02</sub>	8.55 <sup>+0.15</sup> <sub>-0.14</sub>	CB
PG 0052+251	44.75±0.03	5008±73	1.80 <sup>+0.02</sup> <sub>-0.02</sub>	8.77 <sup>+0.11</sup> <sub>-0.11</sub>	CB
PG 0804+761	44.85±0.02	3053±38	1.42 <sup>+0.02</sup> <sub>-0.02</sub>	8.75 <sup>+0.11</sup> <sub>-0.11</sub>	CB
PG 0844+349	44.18±0.07	2694±58	0.96 <sup>+0.04</sup> <sub>-0.04</sub>	7.50 <sup>+0.22</sup> <sub>-0.12</sub>	CB
PG 0921+525	43.62±0.04	1543±5	0.17 <sup>+0.02</sup> <sub>-0.02</sub>	7.63 <sup>+0.13</sup> <sub>-0.26</sub>	CB
	43.69±0.04	1658±3	0.27 <sup>+0.02</sup> <sub>-0.02</sub>	7.70 <sup>+0.14</sup> <sub>-0.14</sub>	CB
	43.47±0.05	1600±39	0.13 <sup>+0.03</sup> <sub>-0.03</sub>	7.16 <sup>+0.12</sup> <sub>-0.12</sub>	CB
PG 0953+414	45.13±0.01	3071±27	1.58 <sup>+0.01</sup> <sub>-0.01</sub>	8.53 <sup>+0.12</sup> <sub>-0.12</sub>	CB
PG 1211+143	44.69±0.08	2012±37	0.98 <sup>+0.05</sup> <sub>-0.05</sub>	8.02 <sup>+0.12</sup> <sub>-0.19</sub>	CB
PG 1226+023	45.90±0.02	3509±36	2.10 <sup>+0.01</sup> <sub>-0.01</sub>	8.96 <sup>+0.12</sup> <sub>-0.12</sub>	CB
PG 1229+204	43.64±0.06	3828±54	0.97 <sup>+0.03</sup> <sub>-0.03</sub>	7.71 <sup>+0.11</sup> <sub>-0.11</sub>	PB
PG 1307+085	44.79±0.02	5059±133	1.83 <sup>+0.03</sup> <sub>-0.03</sub>	8.89 <sup>+0.11</sup> <sub>-0.11</sub>	CB
PG 1351+695	43.64±0.08	5354±32	1.27 <sup>+0.04</sup> <sub>-0.04</sub>	7.35 <sup>+0.11</sup> <sub>-0.11</sub>	PB
PG 1411+442	44.50±0.02	2801±43	1.16 <sup>+0.02</sup> <sub>-0.02</sub>	8.23 <sup>+0.16</sup> <sub>-0.13</sub>	CB
PG 1426+015	44.57±0.02	7113±160	2.01 <sup>+0.02</sup> <sub>-0.02</sub>	9.37 <sup>+0.12</sup> <sub>-0.12</sub>	CB
PG 1434+590	43.73±0.05	4711±49	1.20 <sup>+0.03</sup> <sub>-0.03</sub>	7.39 <sup>+0.11</sup> <sub>-0.11</sub>	PB
	43.61±0.05	5237±67	1.23 <sup>+0.03</sup> <sub>-0.03</sub>	7.61 <sup>+0.11</sup> <sub>-0.12</sub>	PB
	43.61±0.05	4767±72	1.15 <sup>+0.03</sup> <sub>-0.03</sub>	7.81 <sup>+0.13</sup> <sub>-0.13</sub>	PB
PG 1613+658	44.71±0.03	9074±103	2.29 <sup>+0.02</sup> <sub>-0.02</sub>	8.51 <sup>+0.21</sup> <sub>-0.21</sub>	CB
PG 1617+175	44.33±0.02	6641±190	1.82 <sup>+0.03</sup> <sub>-0.03</sub>	8.87 <sup>+0.19</sup> <sub>-0.12</sub>	CB
PG 1700+518	45.53±0.03	2252±85	1.52 <sup>+0.04</sup> <sub>-0.04</sub>	8.95 <sup>+0.14</sup> <sub>-0.13</sub>	CB
PG 2130+099	44.14±0.03	1781±5	0.58 <sup>+0.02</sup> <sub>-0.02</sub>	7.86 <sup>+0.12</sup> <sub>-0.12</sub>	PB
SBS 1116+583A	42.07±0.28	3668±186	0.10 <sup>+0.16</sup> <sub>-0.16</sub>	6.55 <sup>+0.22</sup> <sub>-0.22</sub>	PB

NOTE.— Col. (1): Name. Col. (2): Monochromatic luminosity at 5100 Å for the AGN, corrected for host galaxy light and Galactic extinction. Col. (3): FWHM of broad H $\beta$ , measured from the mean spectrum. Col. (4): Virial product calculated using FWHM. Col. (5): RM-based BH mass, calculated from the H $\beta$  lag, line dispersion of broad H $\beta$ , and  $f = 6.3$  for classical bulges and  $f = 3.5$  for pseudobulges. Col. (6): Bulge type: CB = classical bulge or elliptical; PB = pseudobulge. From compilation of Ho & Kim (2014), which also contains references to original data sources.